Stochastic Analysis of Cascading-Failure Dynamics in Power Grids

Mahshid Rahnamay-Naeini, *Student Member, IEEE*, Zhuoyao Wang, Nasir Ghani, *Senior Member, IEEE*, Andrea Mammoli, *Member, IEEE*, and Majeed M. Hayat, *Fellow, IEEE*

***Abstract*—A scalable and analytically tractable probabilistic model for the cascading failure dynamics in power grids is constructed while retaining key physical attributes and operating characteristics of the power grid. The approach is based upon extracting a reduced abstraction of large-scale power grids using a small number of aggregate state variables while modeling the system dynamics using a continuous-time Markov chain. The aggregate state variables represent critical power-grid attributes, which have been shown, from prior simulation-based and historical-data-based analysis, to strongly influence the cascading behavior. The transition rates among states are formulated in terms of certain parameters that capture grid's operating characteristics comprising loading level, error in transmission-capacity estimation, and constraints in performing load shedding. The model allows the prediction of the evolution of blackout probability in time. Moreover, the asymptotic analysis of the blackout probability enables the calculation of the probability mass function of the blackout size. A key benefit of the model is that it enables the characterization of the severity of cascading failures in terms of the operating characteristics of the power grid.**

***Index Terms*—Blackout probability, cascading failures, Markov chain, power grids, stochastic analysis.**

I. Introduction

WHILE power grids are reliable systems, they have experienced large cascading-failure blackouts at enormous costs. A large number of physical attributes of the power grid, such as voltage and frequency at various points in the grid, power-flow distribution, and the functionality of the grid's components, determine the *state* of the power grid at each time. Various events, such as contingencies, control actions, and demand changes, may alter the state of the system. Cascading failures in power grids can be described as successive changes of power-grid states, for instance, due to component failures, transmission-line tripping, voltage instability, phase mismatch, and changes in power-flow distribution. However, the analytical modeling of the evolution of the detailed system state during cascading failures may not be feasible. This is mainly due the large space of power-grid states and the large number of parameters affecting the states, not to mention the complexity of the interactions between the physical attributes and the stochastic dynamics of states. Besides the physical attributes of the power grid, its operating characteristics (e.g., the power-grid loading level) also affect the interactions among components and the cascading behavior of the power grid. For example, the cascading-failure models reported in [1] and [2] do show that there are critical transitions in the cascading behavior as the load of the system is elevated. Moreover, as power grids become more reliant on the communication and control systems for their daily operation, a new set of operational characteristics pertaining to control and communication systems begin to influence cascading failures [3].

In the past two decades, researchers have exerted considerable efforts in modeling and understanding cascading failures in power systems. Among such efforts is the class of probabilistic models [2], [4]–[7]. However, many of the existing probabilistic models suffer from a disconnect between the parameters of the abstract models they employ and the physical and operating characteristics of the system. We believe that a probabilistic model for cascading failures that exhibits a clear connection between its abstract parameters and the physical and operational characteristics of the system will provide further insight into the cascading behavior.

In this paper, we present an approach that aims to balance the tradeoff that exists between the scalability and analytical tractability of probabilistic models for cascading failures, on the one hand, and the level of details in the description of the physical and operational characteristics that can be embedded in the model on the other hand. Specifically, we construct a scalable and analytically tractable probabilistic model for cascading failure dynamics while retaining certain key physical attributes and operating characteristics of the power grid. This is accomplished by defining a reduced abstraction of the detailed power-grid state space (a small set of equivalence classes) by means of identifying a few aggregate state variables based upon our analysis of power-system simulations and historical data. The aggregate state variables describe the physical attributes of the power-grid states and govern the cascading failure behavior.

Manuscript received June 27, 2013; revised July 16, 2013, October 29, 2013; accepted December 20, 2013. Date of publication January 16, 2014; date of current version June 16, 2014. This work was supported in part by the Defense Threat Reduction Agency's Basic Research Program under Grant HDTRA1-13-1-0020 and the Defense Threat Reduction Agency under Contract DTRA01-03-D-0009-0026, University Partnership Program: Fundamental Research. Paper no. TPWRS-00835-2013.

M. Rahnamay-Naeini, Z. Wang, and M. M. Hayat are with the Department of Electrical and Computer Engineering and Center for High Technology Materials, University of New Mexico, Albuquerque, NM 87131 USA (e-mail: mrahnama@unm.edu; zwang@unm.edu; hayat@unm.edu).

N. Ghani is with the Department of Electrical Engineering, University of South Florida, Tampa, FL 33620 USA.

A. Mammoli is with the Department of Mechanical Engineering, University of New Mexico, Albuquerque, NM 87131 USA.

Color versions of one or more of the figures in this paper are available online at http://ieeexplore.ieee.org.

Digital Object Identifier 10.1109/TPWRS.2013.2297276

The stochastic dynamics of cascading failures are then modeled by the sequence of stochastic transitions among the "abstract" states according to a continuous-time Markov chain. We term the model presented in this paper the *stochastic abstract-state evolution* (SASE) model. The state-dependent transition rates of the SASE model are formulated in terms of the operating characteristics of the power grid including power-grid loading level, transmission-capacity estimation error, and the constraints in implementing load shedding.

The SASE model offers two major contributions beyond existing stochastic models for cascading failures. First, it enables the prediction of the evolution of the blackout probability in terms of key power-grid operating characteristics, which is an expansion of our earlier work [6]. Second, and more importantly, it enables an asymptotic analysis that leads to the analytical characterization of the probability mass function of the blackout size as well as the severity of cascading failures in terms of the key power-grid operating characteristics. We emphasize that the proposed concept of reducing the space of the detailed power-grid states is key in the scalability and analytical tractability of the SASE model.

II. Related Work

In the last two decades, a great volume of work has been devoted to understanding and analyzing cascading failures in power grids (see [8] for a review). Efforts in modeling cascading failures in power grids can be categorized into three classes: analysis of cascading failures using power-system simulations [1], [9], deterministic analytical models [10], and probabilistic analytical models [2], [4]–[7]. Here, we review the probabilistic analytical models for cascading failures.

The work by Brummitt *et al.* [4] and the CASCADE model by Dobson *et al.* [2] model cascading failures triggered by initial load increments on certain components of the system. In both models, failures occur due to overloaded components and the cascading failure develops as a result of redistribution of loads among the remaining components. However, the redistribution of loads are based upon simple assumptions; for example, the CASCADE model assumes loads will be added equally to the components of the system as a result of failures. The probabilistic analytical models based upon branching processes [5], [11], [12] have also emerged, providing an analytical framework to study the statistical properties of cascading failures such as the probability distribution of blackout size. Reported branching-process approaches model cascading failures by considering generations of failures, whereby each failure in each generation independently produces a random number of subsequent failures in the next generation, and so on. In [11] and [12], the authors estimate the failure generation parameter of the branching process model for cascading failures using historical outage datasets. Notably, in [12] the authors account for varying failure generation parameter as the cascade progresses instead of a fixed parameter as in [11]. However, different from the work presented in the current paper, the work in [12] assumes that all line outages are homogeneous in their type.

Recently, we developed a scalable probabilistic approach [6], based upon regeneration theory and a reduced state space of the power grid, to model the dynamics of cascading failures in time. The transition rates among the states of the model are defined to be state- and age-dependent, and they are calculated empirically from power-system simulations. This renewal-based approach can collapse to a Markov process; however, it can also capture the stochastic events when the underlying events are non-Markovian. The independent and concurrent work by Wang *et al.* [7] provides a Markov-transition model for cascading failures. The transition probabilities among states are derived from a stochastic model for line overloading using a stochastic flow redistribution model based upon dc power-flow equations. This model enables simulating the progression of cascading failures and its time span. However, due to the analytical complexity of the time-varying transition probabilities the analytical and asymptotic characterization of probabilistic metrics such as the blackout probability and distribution of the blackout size is not possible. In this paper, we present a scalable probabilistic model for the stochastic dynamics of cascading failures based upon a continuous-time Markov chain framework that captures key physical attributes of the power grid through its parameters and the novel definition of its reduced state space.

III. Abstract State Space of Power Grids

Our power-system simulations [6], as well as available historical blackout data [13]–[15], all suggest that the functionality status of transmission lines and their power-flow capacities [16] are key physical attributes that should be considered in modeling cascading failures. The importance of these attributes are clear as line failures have always been a part of historical large blackouts and the capacity of transmission lines determine the power-delivery capacity of the grid. For simplicity, we term the nonfunctional lines (e.g., lines that are tripped by protection relays, overheated, or physically failed) the *failed lines*. Even in the case where only the functionality status of the m transmission lines of the system are considered, the size of the state space of the power grid is exponential in m.

We consider three aggregate state variables to represent the power-grid state. The first variable is the number of failed lines, F, which has been commonly considered in the probabilistic modeling of cascading failures to represent power-grid states [1], [5], [7], [12]. Next, we consider the maximum of the capacities of all of the failed lines, $C^{\max}$. Our simulations presented in [6] have shown that $C^{\max}$ dominates the effect of the capacity of the failed lines in cascading failures. Finally, our simulations presented in [6] have shown that certain power-grid states are *cascade-stable*, defined as a state for which once entered no further failures occur in the system. Accordingly, we define a new aggregate state variable, termed cascade-stability, which collectively captures many other physical attributes of the power grid (as the physical attributes specify whether a power-grid state is cascade-stable or not). We represent the cascade-stability by a binary state variable I, where $I = 1$ indicates a cascade-stable state and $I = 0$ indicates otherwise.

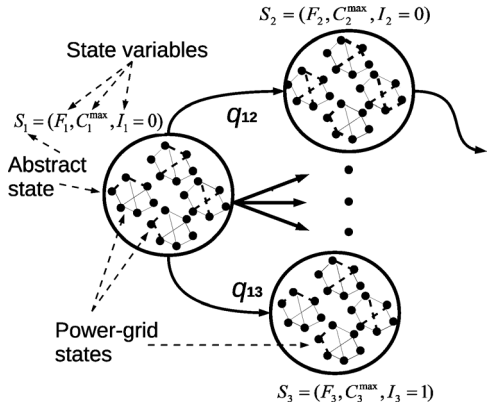

Fig. 1. Power-grid states, abstract states, and transitions between the abstract states.

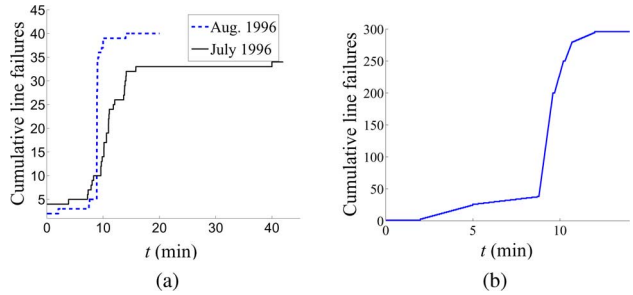

Fig. 2. Cumulative line failures in the (a) July 1996 WSCC blackout (solid line), August 1996 WSCC blackout (dashed line), and (b) August 2003 blackout [13], [15]. The time of the initial failure is set to zero. The figures are reproduced in the same way as in [5].

Here, we employ an expanded notion of equivalence classes of power-grid states compared to what we originally proposed in [6]. By utilizing the three introduced state variables as the descriptors of power-grid states, we partition the space of all detailed power-grid states into a collection of equivalence classes, denoted by $\mathcal{S}$. Such coarse partitioning of the state space of the power grid implies that detailed power-grid states with the same aggregate state-variable values (i.e., the same value of $F, C^{\max}$ and I) will belong to one class and will be indistinguishable as far as the reduced abstraction is concerned. We term each class of the power-grid states an *abstract power-grid state* or in short an *abstract state*, and label each as $S_i = (F_i, C_i^{\max}, I_i)$, where $S_i \in \mathcal{S}$.

The notion of power-grid states, abstract states, and transition between the abstract states is sketched in Fig. 1. Each large circle represents an abstract state and each of the four topological graphs inside each large circle represents a detailed power-grid state, albeit with common values for $F, C^{\max}$ and I. We assume that the power-flow capacity of the lines can be quantized into a discrete and finite set of capacity values, i.e., $\mathcal{C} = \{C_1, C_2, \ldots, C_K\}$. Thus, the cardinality of the abstract-state space $\mathcal{S}$ is $N = 2Km$. Therefore, the equivalence-class approach reduces the complexity associated with tracking the stochastic dynamics of the power grid from exponential to linear in m.

Next, we provide two real scenarios of cascading failures from the historical blackout data that support the dependency of the cascading behavior on F and $C^{\max}$. The time evolution of the cumulative line failures for the blackouts in July 1996 and August 1996 in the Western Interconnection [13] are shown in Fig. 2(a). The number of initial and final transmission-line failures are very close in these two blackouts. However, the approximate average line-failure rate in the July 1996 blackout is 1.6 failures per minute during the escalation phase of the cascading failures, while it is 4 failures per minute in the August 1996 blackout. Most notably, the initial disturbance of the blackouts were two 345-KV transmission-line failures in the July 1996 blackout and two 500-KV transmission-line failures in the August 1996 blackout. Next, the time evolution of the cumulative line failures for the blackout in the August 2003 in Eastern Interconnection [15] is shown in Fig. 2(b). Based upon the data, the average line-failure rate is approximately 1.4 failures per minute at the beginning phase while it is 18 failures per minute at the escalation phase of cascading failures. This can be described by the larger number of failures in the grid in the second phase as well as failure of some critical lines with high capacities. In summary, the aforementioned observations extracted from historical data and our simulations both support the selection of the capacity of the failed lines and the number of failures as key players in the formulation of the abstract state space.

IV. SASE Cascading-Failure Model

The SASE model describes the stochastic dynamics of cascading failures using a finite state continuous-time Markov chain whose state space is defined by the abstract states $S_i = (F_i, C_i^{\max}, I_i)$ for $i = 1, 2, \ldots, N$. Recall that the state variable I indicates whether a state is cascade-stable or not; hence, it is utilized to specify the *absorbing* $(I = 1)$ and *nonabsorbing* $(I = 0)$ states of the Markov chain. We term the nonabsorbing states as transitory states.

We consider two types of state transitions in the SASE model. The first type is termed as *cascade-stop* transition, which is from a transitory state, say S_i, to an absorbing state, say S_j, (i.e., $I_i = 0$ and $I_j = 1$) such that $F_j = F_i$ and $C_j^{\max} = C_i^{\max}$. The cascade-stop transition leads to the end of the chain of failures, which in real systems can occur as a result of the implementation of successful control actions, formation of operating islands in the power grid, or occurrence of a large blackout. The second type of transitions is termed a *cascade-continue* transition. We assume that the cascade-continue transition occurs as a result of a single line failure in the system. The single-failure-per-transition approximation is based upon the assumption that time is divided into sufficiently small intervals such that each interval can allow only a single failure event. By *cascade-continue transition* we mean transition from a transitory state, say S_i, to another transitory state, say S_j (i.e., $I_i = I_j = 0$) such that $F_j = F_i + 1$ and $C_j^{\max} \geq C_i^{\max}$. To this end, the cascading failure can be described as a sequence of Markovian transitions among transitory states with a final transition to some absorbing state.

We represent the state of the system at time $t \geq 0$ by $X(t)$, an $\mathcal{S}$-valued, continuous-time Markov chain. The transition probability matrix of the chain $X(t)$ is denoted by $\mathbf{P}(t)$, where its ijth element is $p_{ij}(t) = \mathsf{P}\{X(\tau + t) = S_j \mid X(\tau) = S_i\}, t \geq 0$. Note that the notation P is used to represent probability measure

defined on the collection (σ-algebra) $\mathcal{F}$ of all events (subsets of the sample space Ω) generated by the random variables defined in this paper.

Let q_{ij} for $i \neq j$ represent the probability rate of transition from state S_i to state S_j, which depends upon the origin and destination states of the transition. This dependency allows for cascading behavior and will be explained in details in Section VI. The q_{ij} is defined as

$$q_{ij} = \begin{cases} \lim_{h\to 0^+} \frac{p_{ij}(h)}{h}, & \text{for } i \neq j \\ -\lim_{h\to 0^+} \frac{1-p_{ij}(h)}{h}, & \text{for } i = j \end{cases} \quad (1)$$

where q_{ii} satisfies $q_{ii} = -\sum_{j=1, j\neq i}^{N} q_{ij}$ [17]. A Markov chain $X(t)$ is completely determined by the transition rate matrix $\mathbf{Q}$ with q_{ij} as its ijth element.

We formulate the transition rates of the SASE model based upon the transition probabilities of its embedded Markov chain (EMC). We denote the state of the EMC at discrete time instant ℓ by $X^{(\ell)}$. The one-step transition probability matrix of the EMC is denoted by $\mathbf{P}^{\mathrm{EMC}}$. According to the definition of the SASE model, the elements of $\mathbf{P}^{\mathrm{EMC}}$ has the form given in (2), shown at the bottom of the page, where $P_{\mathrm{trans}}(S_i, S_j)$ represents the probability that the system transits from a transitory state, say S_i, to state S_j for which the value of F_j and $C_j^{\max}$ does not violate the transition rules in (2). In Section VI, we will parametrically characterize $P_{\mathrm{trans}}(S_i, S_j)$ based upon our observations from simulations.

We approximate q_{ij} based upon (1) and for a small Δt as $q_{ij} \approx (p_{ij}^{\mathrm{EMC}})/(\Delta t)$ for $i \neq j$. We consider Δt as (the small) unit of time approximating the average time between failures during the rapid escalation phase of the cascading behavior, which is relatively small compared with the total duration of cascading failures. We estimate such Δt using the historical blackout data provided in [5] and [13]. However, note that, based upon the individual blackout events, Δt may vary depending on the power system and its operating characteristics. For example, historical data suggests approximately 18 transmission-line failures per minute on average during the rapid escalation phase of the cascading failure for the August 2003 Eastern Interconnection blackout ($\Delta t \approx$ 0.055 min) [13] while this number is 4 failures per minute for the August 1996 Western Interconnection blackout ($\Delta t \approx$ 0.25 min) [5]. In our calculations we have selected an intermediate value of $\Delta t =$ 0.1 min. We emphasize that, while we consider a fixed Δt for the system, it is the state-dependent nature of the transition probabilities p_{ij}^{EMC} that inherently adjusts the transition rates to accommodate all phases of cascading failures, such as the precursor and escalation phases.

In Section V, we introduce our simulation methodology, which will be used in the parametric formulation of p_{ij}^{EMC}.

V. Cascading-Failure Simulation

A. Overloading and Failure Mechanism

Here, we introduce our approach for simulating cascading failures resulting from line overloading. Our simulations are based upon the dc power-flow equations as described in [18].

A transmission line has a power-flow capacity that can be governed by the thermal limit, the voltage drop limit, or the steady-state stability limit of the line [16]. We denote the power-flow capacity of a transmission line, say the kth line, by C_k^{opt}. The C_k^{opt} values of the transmission lines are used by the control center of the power grid as constraints in the power-flow optimization framework (presented in Section V-C).

Similarly to the approach presented in [1], we consider a threshold α_k for the power flow through the kth line above which the protection relay (e.g., circuit breaker or impedance protective relay) trips the line. Various factors and mechanisms in the power grid may affect the threshold α for transmission lines. For example, the line overloading may lead to smaller measured impedance than relay settings [19], the thermal power-flow capacity of a transmission line may vary due to changes in the surrounding temperature and ambient weather conditions [20], or communication/control system problems may lead to inaccurate C_k^{opt} assumption in the control center. In all of these examples, the protection relay may trip the line when the power flow exceeds the threshold α_k. Now, one may interpret the discrepancy between the threshold value α_k, which represents the true capacity of the line, and the nominal capacity C_k^{opt} as an error by the control center in its estimation of the true capacity of the lines. By adopting this point of view, in this paper, we term $C_k^{\mathrm{opt}} - \alpha_k$ the capacity estimation error. While the approach presented in [1] considers a fixed threshold, in this paper we assume varying threshold to capture the effects of various parameters on the threshold and consequently on the cascading behavior. In our simulations, we quantify $C_k^{\mathrm{opt}} - \alpha_k$ by a fraction of C_k^{opt}, i.e., $C_k^{\mathrm{opt}} - \alpha_k = eC_k^{\mathrm{opt}}$ for $e \in [0, 0.5]$. Therefore, we assume a line is overloaded when the power flow through the line exceeds $(1-e)C_k^{\mathrm{opt}}$. As such, the parameter e controls the capacity estimation error. Moreover, we categorize all of the transmission lines in the power grid based upon their capacity values into five categories with values from the set $\mathcal{C} = \{20\text{ MW}, 80\text{ MW}, 200\text{ MW}, 500\text{ MW}, 800\text{ MW}\}$ [16]. Similarly to the work presented in [21], in our simulations, we allow only one line trip at a time by randomly (according to the size of overload) tripping one of the overloaded lines.

Studies of major blackouts have shown that incorrect operation of protection relays contributes to cascading failures [13]. To capture this effect in our simulations, we have considered a small probability (0.04) for mis-operation of protection relays. Due to space constraints, we will not investigate the effects of

$$p_{ij}^{\mathrm{EMC}} = \begin{cases} 0, & F_j < F_i \text{ or } F_j - F_i > 1 \text{ or } C_j^{\max} < C_i^{\max} \text{ or } (I_i = 1 \text{ and } j \neq i) \\ 1, & I_i = 1 \text{ and } j = i \\ P_{\mathrm{trans}}(S_i, S_j), & \text{otherwise} \end{cases} \quad (2)$$

the mis-operation of the protection relays on cascading behavior further. A study of such effects is presented in [22]. Finally, the simulations in this paper use the IEEE 118-bus system. However, we also refer to our simulations of IEEE 300-bus system for certain results to confirm the consistency of the observed trends.

B. Operating Characteristics of the Power Grid

In studying the cascading failures, we consider three power-grid operating characteristics as described below.

Capacity Estimation Error: Recall that in the previous subsection we introduced the parameter e, which captures the effects of various factors and mechanisms that may lead to failure of transmission lines when their power flow is within a certain range of the maximum (nominal) capacity assumed by the control center. We use the parameter e to control the capacity estimation error (as described in the previous subsection).

Power-Grid Loading Level: We denote the power-grid loading level by r, which is defined as the ratio of the total demand to generation-capacity of the power grid. The parameter r represents the level of stress over the grid in terms of the loading level of its components. Note that the *N-1* security is ensured in all loading levels of the power grid.

Load-Shedding Constraint Level: Load shedding is a critical control action when the system must be reconfigured to accommodate the disturbances on the power grid. In our earlier work [23], we have shown that the efficiency of the load shedding in responding to cascading failures depends upon the constraints in implementing the load shedding in the system. The constraint level is governed, for example, by control and marketing policies, regulations, physical constraints, and communication limitations. The ratio of the uncontrollable loads (loads that do not participate in load shedding) to the total load in the power grid is termed the *load-shedding constraint*, denoted by $\theta \in [0, 1]$, where $\theta = 1$ means load shedding cannot be implemented and $\theta = 0$ means there is no constraint in implementing the load shedding. The value of θ controls the level of controllability of the load shedding in our simulations.

The effects of these parameters on the power-flow distributions are embedded in the power-flow optimization framework as described in Section V-C.

C. Power-Flow Optimization Framework

For completeness, we summarize the power-flow optimization framework, introduced in our earlier work [3], [23].

Consider the transmission system of a power grid with $\mathcal{V}$ nodes (substations) interconnected by m transmission lines. The sets $\mathcal{L}$ and $\mathcal{G}$ are the set of load buses and the set of generator buses, respectively. The notation L_i represents the demand at the load bus i. The dc power-flow equations [18] can be summarized as

$$\tilde{F} = A\tilde{P} \tag{3}$$

where $\tilde{P}$ is a power vector whose components are the input power of nodes in the grid (except the reference generator), $\tilde{F}$ is a vector whose m components are the power flow through the transmission lines, and A is a matrix whose elements can be calculated in terms of the connectivity of transmission lines in the power grid and the impedance of the lines. This system of equations does not have a unique solution. Therefore, to find the solution to this system, we use, as done in [1], a standard optimization approach with the objective of minimizing the simple cost function that follows:

$$\text{Cost} = \sum_{i \in \mathcal{G}} w^g{}_i g_i + \sum_{j \in \mathcal{L}} w^\ell{}_j \ell_j. \tag{4}$$

A solution to this optimization problem is the pair g_i and ℓ_j that minimizes the cost function in (4). Note that $\ell_j = \theta_j L_j + b_j$, where b_j will be determined by the optimization solution. In this cost function, $w^g{}_i$ and $w^\ell{}_j$ are positive values representing the generation cost for every node $i \in \mathcal{G}$ and the load-shedding price for every node $j \in \mathcal{L}$, respectively. We assume a high price for load shedding so that a load is to be curtailed only when there is generation inadequacy or transmission capacity limitations. The constraints for this optimization problem are listed here.

1) DC power flow equations: $\tilde{F} = A\tilde{P}$.
2) Limits on the generators' power: $0 \le g_i \le G_i{}^{\max}, i \in \mathcal{G}$.
3) Limits on the controllable loads: $(1-\theta_j)L_j \le b_j \le 0, j \in \mathcal{L}$.
4) Limits on the power flow through the lines: $|\tilde{F}_k| \le C_k^{\text{opt}}$ for $k \in \{1, \ldots, m\}$.
5) Power balance constraints (power generated and consumed must be balanced): $\sum_{i \in \mathcal{G}} g_i + \sum_{j \in \mathcal{L}} \ell_j = 0$.

Note that, in the above formulation, the quantities ℓ_j are negative and the g_i's are positive (by definition). The operating parameter r affects the initial load on the system, i.e., the L_j's. The solution to this optimization problem determines the amount of load shed, generation, and the power flow through the lines. If failures occur in the power grid, we assume that the control center redistributes the power in the grid by solving the above optimization problem. If the new power-flow distribution overloads lines (based on the overload definition in Section V.A), more failures will occur in the power grid. This process iterates until no more failures occur in the system.

We use MATPOWER [24], which is a package of MATLAB m-files, for solving the optimal power flow and simulating cascading failures. The quasi-static approaches that employ a power-flow distribution framework together with a method to identify overloaded lines and individual failures to model cascading failures have been used in several works in the literature such as [19], [21], and [25]. In Section VI, we will use simulations to study the effects of the three introduced power-system operating characteristics on cascading failures and use this understanding to parametrically formulate p_{ij}^{EMC}.

VI. Transition Probabilities

Here, we parametrically model $P_{\text{trans}}(S_i, S_j)$ introduced in (2). In order to simplify the formulation of the $P_{\text{trans}}(S_i, S_j)$, we consider the probability components depicted in Fig. 3. We will introduce the components represented in Fig. 3 as we go through this section and refer to this figure as necessary.

Note that, for every transitory state, say $S_i \in \mathcal{S}$, there is a single associated absorbing state, which we denote by S_i^* (see Fig. 3). Note that state S_i^* has the same F and $C^{\max}$ values as those for S_i but it has $I_i^* = 1$ (where as $I_i = 0$). Based upon

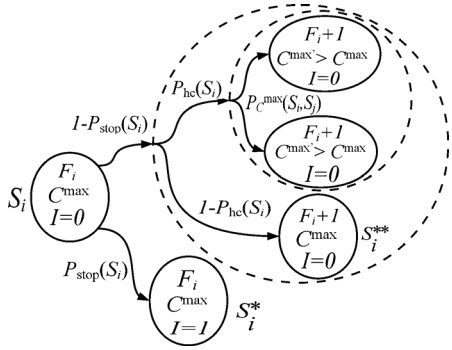

Fig. 3. Components of $P_{\text{trans}}(S_i, S_j)$. First, transition from a transitory state S_i is divided into two categories: transition to an absorbing state S_i^* and transition to a transitory state (states in the dashed circles are transitory states). Next, the transition to a transitory state is also divided into two categories: transition to a state S_i^{**} with the same $C^{\max}$ values as that of S_i, and transition to a state whose maximum capacity of the failed lines is larger than $C^{\max}$ associated with the state S_i.

whether the next state of the transition is an absorbing state or not, we decompose the transition probability as follows:

$$\begin{aligned} &P_{\text{trans}}(S_i, S_j) \\ &\quad = \mathsf{P}\left\{ X^{(\ell+1)} = S_j \middle| X^{(\ell)} = S_i, X^{(\ell+1)} = S_i^* \right\} \\ &\qquad \times \mathsf{P}\left\{ X^{(\ell+1)} = S_i^* \middle| X^{(\ell)} = S_i \right\} \\ &\qquad + \mathsf{P}\left\{ X^{(\ell+1)} = S_j \middle| X^{(\ell)} = S_i, X^{(\ell+1)} \neq S_i^* \right\} \\ &\qquad \times \mathsf{P}\left\{ X^{(\ell+1)} \neq S_i^* \middle| X^{(\ell)} = S_i \right\}. \end{aligned} \tag{5}$$

Note that $X^{(\ell+1)} = S_i^*$ implies that cascading failure ends in the system. As such, we define the probability of cascade-stop transition as $P_{\text{stop}}(S_i) \triangleq \mathsf{P}\{X^{(\ell+1)} = S_i^* \,|\, X^{(\ell)} = S_i\}$. Clearly, $\mathsf{P}\{X^{(\ell+1)} = S_j \,|\, X^{(\ell)} = S_i, X^{(\ell+1)} = S_i^*\} = \delta_{S_i^*,S_j}$, where $\delta_{S_i^*,S_j} = 1$ when S_j is equal to S_i^* and $\delta_{S_i^*,S_j} = 0$ otherwise. Moreover, we define $\mathsf{P}\{X^{(\ell+1)} = S_j \,|\, X^{(\ell)} = S_i, X^{(\ell+1)} \neq S_i^*\} \triangleq (1 - \delta_{S_i^*,S_j}) P_{\text{cont}}(S_i, S_j)$, where $P_{\text{cont}}(S_i, S_j)$ is the conditional cascade-continue transition probability. Thus, we rewrite (5) as

$$\begin{aligned} P_{\text{trans}}(S_i, S_j) =& \delta_{S_i^*,S_j} P_{\text{stop}}(S_i) \\ &+ (1 - \delta_{S_i^*,S_j}) P_{\text{cont}}(S_i, S_j)(1 - P_{\text{stop}}(S_i)) \end{aligned} \tag{6}$$

for $S_i, S_i^*, S_j \in \mathcal{S}$. Note that $\sum_{j=1}^{N} P_{\text{trans}}(S_i, S_j) = 1$.

The rest of this section is devoted to the parametric representation of $P_{\text{stop}}(S_i)$ and $P_{\text{cont}}(S_i, S_j)$, and therefore, the parametric formulation of $P_{\text{trans}}(S_i, S_j)$ due to (6).

A. Cascade-Stop Probability

Here, we will present simulation results that show the dependency of $P_{\text{stop}}(S_i)$ on F_i and $C_i^{\max}$. To simplify the observation of the effects of F_i and $C_i^{\max}$ on $P_{\text{stop}}(S_i)$, we have studied $P_{\text{stop}}(S_i)$ as a function of F_i and $C_i^{\max}$ individually represented, respectively, by $P_{\text{stop}}^{(1)}(F_i)$ and $P_{\text{stop}}^{(2)}(C_i^{\max})$. In Appendix A, we present a simple approach similar to the approach presented in [26] in conjunction with certain reasonable

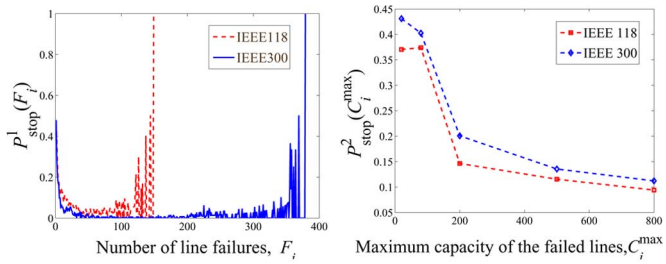

Fig. 4. (a) $P_{\text{stop}}^{(1)}(F_i)$ and (b) $P_{\text{stop}}^{(2)}(C_i^{\max})$ for the IEEE 118-bus system and the IEEE 300-bus system for $r = 0.7$, $e = 0.1$, and $\theta = 0$.

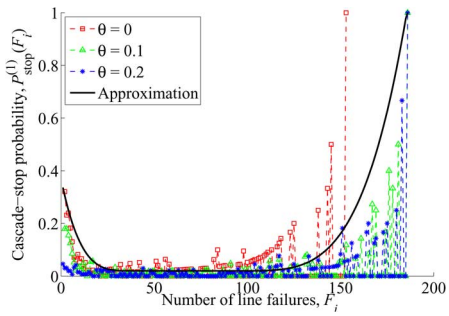

Fig. 5. Simulation results of $P_{\text{stop}}^{(1)}(F_i)$ for $r = 0.7$, $e = 0.1$ and three values of θ. The solid line is the parametric approximated function when $\theta = 0$.

assumptions (originated from the simulations of the power grid and power grid characteristics) to approximately represent $P_{\text{stop}}(S_i)$ in terms of a weighted superposition of $P_{\text{stop}}^{(1)}(F_i)$ and $P_{\text{stop}}^{(2)}(C_i^{\max})$ as

$$P_{\text{stop}}(S_i) = w P_{\text{stop}}^{(1)}(F_i) + (1 - w) P_{\text{stop}}^{(2)}(C_i^{\max}) \tag{7}$$

where, in our formulation, we simply set $w = 0.5$.

Fig. 4(a) and (b) shows the simulation results of $P_{\text{stop}}^{(1)}(F_i)$ and $P_{\text{stop}}^{(2)}(C_i^{\max})$, respectively, for the IEEE 118-bus and the IEEE 300-bus systems. The IEEE 118-bus system has 186 transmission lines and the IEEE 300-bus systems has 409 transmission lines. Note that $P_{\text{stop}}^{(1)}(F_i)$ and $P_{\text{stop}}^{(2)}(C_i^{\max})$ exhibit the same general behavior in both grids. Due to the space constraints, we will limit our presentation to the IEEE 118-bus system with the knowledge that a similar approach for the parametric modeling of transmission rates can be applied to larger scale grids by adjusting the parameters of the model.

Figs. 5 and 6 show the simulation results of $P_{\text{stop}}^{(1)}(F_i)$ and $P_{\text{stop}}^{(2)}(C_i^{\max})$ for the IEEE 118-bus system, respectively, for different operating settings of the grid. The results of our simulations are obtained using 1000 scenarios of random initial disturbances with two or three random line failures. We considered three different values of load-shedding constraint level θ in order to show that operating characteristics of the power grid affect the stability probabilities while the value of r and e are fixed to be 0.7 and 0.1, respectively (the effects of r, and e are discussed in Section VI-C).

From Fig. 5, we observe that $P_{\text{stop}}^{(1)}(F_i)$ is bowl-shaped, with three identifiable phases, which are described in detail below. The importance of the bowl-shape form is that it reflects the general cascading behavior as failures accumulate. A similar

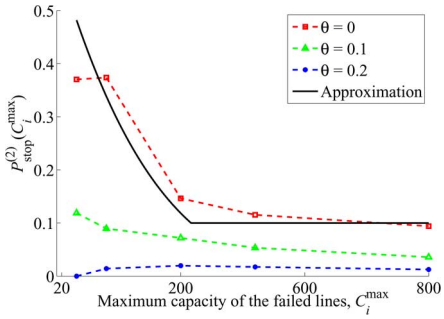

Fig. 6. Simulation results of $P^{(2)}_{\text{stop}}(C_i^{\max})$ for $r = 0.7, e = 0.1$ and three values of θ. The solid line is the parametric approximated function when $\theta = 0$.

three-phase behavior can be observed in the historical cascading-failure data presented in Fig. 2.

First Phase: This phase represents the regime when the likelihood of an additional failure increases substantially as a function of the number of failures. A qualitatively similar increase in the failure propagation probability has also been observed by Dobson [12]. This phase starts at $F_i = 2$ (due to *N-1* security). To this end, we define the parameter a_1 as $P^{(1)}_{\text{stop}}(2)$, which represents, intuitively speaking, the reliability of the power grid to initial disturbances with two failures. Also in the first phase, $P^{(1)}_{\text{stop}}(F_i)$ decreases from a_1 to a small $P^{(1)}_{\text{stop}}(F_i)$ value, ϵ (our results suggest $\epsilon = 0.05$), as the number of failures increases and reaches a critical $F_i = a_2 m$ value.

Second Phase: This phase represents the escalated phase of cascading failures. During this phase $P^{(1)}_{\text{stop}}(F_i)$ is small (we assume $P^{(1)}_{\text{stop}}(F_i) = \epsilon$ during this phase) and the power grid is highly vulnerable. This phase starts at $F_i = a_2 m$, which represents the number of failures in the power grid after which the cascading failure enters the escalated phase. As expected, our results show that, during this phase, the efficiency of the control action (represented by θ) hardly affects $P^{(1)}_{\text{stop}}(F_i)$.

Third Phase: As F_i increases further, the probability of having an additional failure decreases as cascading-failure behavior begins to phase out. This behavior can be attributed to the finite size of the power grid or the fact that as more failures occur "functional islands" may form in the grid, leading to the termination of cascading failures. Therefore, in this phase, the value of $P^{(1)}_{\text{stop}}(F_i)$ rises, and, finally, $P^{(1)}_{\text{stop}}(m) = 1$. Note that, in this paper, we simply consider a fixed parametric model for the third phase of $P^{(1)}_{\text{stop}}(F_i)$, which only roughly approximates the average scenario of various operating settings.

We propose the following parametric model to capture the three aforementioned phases in $P^{(1)}_{\text{stop}}(F_i)$:

$$P^{(1)}_{\text{stop}}(F_i) = \begin{cases} a_1 \left(\frac{a_2 m - F_i}{a_2 m}\right)^4 + \epsilon, & 2 \le F_i \le a_2 m \\ \epsilon, & a_2 m < F_i \le 0.6m \\ \min\left\{\left(\frac{F_i - 0.6m}{m - 0.6m}\right)^4 + \epsilon, 1\right\}, & 0.6m < F_i \le m. \end{cases} \quad (8)$$

The parametric $P^{(1)}_{\text{stop}}(F_i)$ is shown in Fig. 5 for $\theta = 0$. Recall that we have judiciously selected a common parametric model for the third phase of the bowl-shaped function across various operating settings. Consequently, the parametric function $P^{(1)}_{\text{stop}}(F_i)$ shown in Fig. 5 does not accurately match the simulation results for $\theta = 0$ scenario in the third phase.

The empirically calculated $P^{(2)}_{\text{stop}}(C_i^{\max})$ is shown in Fig. 6. The value of $P^{(2)}_{\text{stop}}(C_i^{\max})$ indicates, intuitively speaking, the reliability of the power grid when the maximum capacity of the failed lines in the grid is $C_i^{\max}$. Note that $P^{(2)}_{\text{stop}}(C_i^{\max})$ decreases as $C_i^{\max}$ increases, which means that the power grid is more vulnerable to additional failures when it has lost at least a line with a large capacity value. We also observe that $P^{(2)}_{\text{stop}}(C_i^{\max})$ decreases for all $C_i^{\max}$ values as θ increases; however, the effect of θ on the reliability is larger when $C_i^{\max}$ is smaller. This is because control actions are most effective when they are implemented in the beginning phase of cascading failures where $C^{\max}$ is more likely to be small.

The $P^{(2)}_{\text{stop}}(C_i^{\max})$ is formulated parametrically as

$$P^{(2)}_{\text{stop}}(C_i^{\max}) = \max\left\{a_3 \left(\frac{C_i^{\max} - \max\{\mathcal{C}\}}{\max\{\mathcal{C}\}}\right)^4, a_4\right\} \quad (9)$$

where $a_3 \triangleq P^{(2)}_{\text{stop}}(\min\{\mathcal{C}\})$ and $a_4 \triangleq P^{(2)}_{\text{stop}}(\max\{\mathcal{C}\})$. The parametric function of $P^{(2)}_{\text{stop}}(C_i^{\max})$ is also shown (by the solid line) in Fig. 6. This completes the parametric modeling of $P_{\text{stop}}(S_i)$ based on (7). In Section VI-C, we show that the value of $a_1, \ldots, a_4$ are affected by r, e, and θ. In the SASE model, we will perceive the parameters $a_1, \ldots, a_4$ beyond abstract model parameters but as parameters that govern the cascading behavior while maintaining a physical connection to the operating characteristics of the system.

B. Cascade-Continue Probability

Recall that, for every transitory state S_i, there is only one transitory state with the same $C^{\max}$ as that of state S_i and exactly one more failure than that for state S_i. We denote such state by S_i^{**} (see Fig. 3). Failure of a line with capacity smaller than or equal to $C_i^{\max}$ results in transitioning from state S_i to state S_i^{**}. Similarly to (5), depending on whether the next line failure has larger capacity than $C_i^{\max}$ or not, we can write the conditional cascade-continue transition probability by conditioning on S_i^{**} as

$$\begin{aligned} P_{\text{cont}}(S_i, S_j) =& (1 - P_{\text{hc}}(S_i))\delta_{S_i^{**}, S_j} \\ &+ (1 - \delta_{S_i^{**}, S_j}) P_{C^{\max}}(S_i, S_j) P_{\text{hc}}(S_i) \end{aligned} \quad (10)$$

for $S_i, S_i^{**}, S_j \in \mathcal{S}$ and $I_j = 0$, where P_{hc} is defined as the probability of having a line failure that results in a higher capacity of the failed lines than $C_i^{\max}$. In (10), $P_{\text{hc}}(S_i) \triangleq \mathsf{P}\{X^{(\ell+1)} \neq S_i^{**} \,|\, X^{(\ell)} = S_i, X^{(\ell+1)} \neq S_i^*\}$ and $(1 - \delta_{S_i^{**}, S_j}) P_{C^{\max}}(S_i, S_j) \triangleq \mathsf{P}\{X^{(\ell+1)} = S_j \,|\, X^{(\ell)} = S_i, X^{(\ell+1)} \neq S_i^{**}, X^{(\ell+1)} \neq S_i^*\}$.

The empirically calculated $P_{\text{hc}}(S_i)$ as a function of F_i and $C_i^{\max}$ is shown in Fig. 7 with the same simulation settings as that of the previous subsection. Our simulation results show strong evidence that F_i and $C_i^{\max}$ affect $P_{\text{hc}}(S_i)$. Results suggest that regardless of the $C_i^{\max}$ value of the power-grid state, as F_i increases the probability that a line with capacity larger than $C_i^{\max}$ fails increases. This is meaningful because, as the

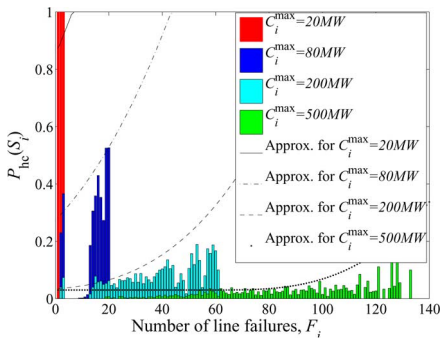

Fig. 7. Simulation results of $P_{\rm hc}(S_i)$ as a function of F_i and $C_i^{\max}$ for $r = 0.7, e = 0.1$ and $\theta = 0.1$.

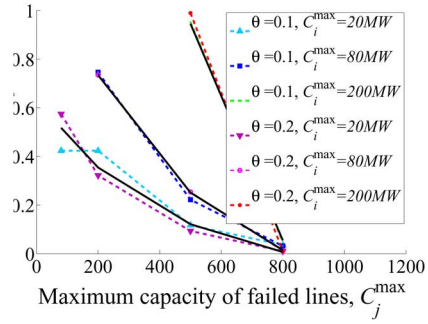

Fig. 8. Simulation results of $P_{C^{\max}}(S_i, S_j)$ as a function of $C_i^{\max}$ and $C_j^{\max}$ for $r = 0.7$ and $e = 0.1$ and two values of θ. The parametric approximations are represented by solid lines.

number of failures increases the power grid becomes vulnerable and hence large transmission lines may be affected by contingencies. Moreover, the ratio of the number of transmission lines with capacity larger than $C_i^{\max}$ to the total number of functional lines increases with F_i. The next general observation from Fig. 7 is that for the same F_i value, as $C_i^{\max}$ increases the probability that a line with capacity larger than $C_i^{\max}$ fails decreases. This is mainly due to decrease in the number of lines with capacity value larger than $C_i^{\max}$ (as $C_i^{\max}$ increases). Furthermore, it is less likely to have states with $C_i^{\max}$ value after F_i reaches a certain threshold denoted by Γ_i (the value of Γ_i increases as $C_i^{\max}$ increases). This means that as F_i approaches Γ_i, line failures with capacity larger than $C_i^{\max}$ become highly likely.

Based upon our simulations, the role of θ, r and e in $P_{\rm hc}(S_i)$ is subtle. Therefore, in this paper, we approximate $P_{\rm hc}(S_i)$ for different operating characteristics of the power grid with a fixed function. The above trends in $P_{\rm hc}(S_i)$ are captured by

$$P_{\rm hc}(S_i) = \begin{cases} \alpha(F_i + \beta)^3, & 2 \le F_i \le \Gamma_i \\ 1, & \Gamma_i < F_i \end{cases} \tag{11}$$

for $S_i \in \mathcal{S}$, where $\alpha = 6 \times 10^{-7}$ and β is $C_i^{\max}$ dependent. The parametric $P_{\rm hc}(S_i)$'s are shown in Fig. 7. Note that the overestimation of the curves in Fig. 7 is due to employing a common parametric model for various operating settings as well as the introduced parameter Γ_i (there are no simulation data when F_i is beyond Γ_i.)

Next, we find the parametric formulation for $P_{C^{\max}}(S_i, S_j)$. Our simulation results suggest that $C_i^{\max}$ and $C_j^{\max}$ play key roles in determining $P_{C^{\max}}(S_i, S_j)$. Fig. 8 shows the empirically calculated $P_{C^{\max}}(S_i, S_j)$ as a function of $C_i^{\max}$ and $C_j^{\max}$. From Fig. 8, we observe that, conditional on the occurrence of an additional failure with capacity larger than $C_i^{\max}$, the probability of transitioning to state S_j decreases as $C_j^{\max}$ increases. The results suggest that lines with capacity value close to $C_i^{\max}$ have a higher probability of failure than those with much larger capacities than $C_i^{\max}$. We also observe that the probability of transitioning to state S_j increases as $C_i^{\max}$ increases. This is because the power grid becomes more vulnerable when $C_i^{\max}$ is large. By comparing the simulation results corresponding to two values of θ in Fig. 8, we conclude that the role of θ in $P_{C^{\max}}(S_i, S_j)$ is also subtle and, similarly to $P_{\rm hc}(S_i)$, the effect of operating characteristics on $P_{C^{\max}}(S_i, S_j)$ is not considered.

To capture the described trends, $P_{C^{\max}}(S_i, S_j)$ is modeled parametrically as

$$P_{C^{\max}}(S_i, S_j) = \frac{w(C_j^{\max})}{\sum\limits_{k:C_k > C_i^{\max}} w(C_k)} \tag{12}$$

where $w(C_k)$ is what we term the weight of transition to a state with the maximum capacity of the failed line equal to C_k. We have assigned these weights such that they approximate the simulation results presented in Fig. 8 using (12). Here, the value of the weights are set to $w(80\ \text{MW}) = 2.2$, $w(200\ \text{MW}) = 1.5$, $w(500\ \text{MW}) = 0.5$, and $w(1500\ \text{MW}) = 0.01$. This completes the modeling of $p_{ij}^{\rm EMC}$ presented in (2).

C. Effects of Operating Characteristics on SASE Parameters

The SASE model parameters $a_1, \ldots, a_4$ determine different cascading behaviors. These parameters may vary under different operating conditions and also across different power grids due to different connectivity pattern and components characteristics. Recall that we made the general observation that the power grid is more reliable when $a_1, \ldots, a_4$ are larger. To illustrate the effects of operating characteristics on $a_1, \ldots, a_4$, the values of these parameters (obtained based upon simulation results) are shown in Figs. 9 and 10 for different θ, r and e values. Our simulation results suggest that the power grid is more reliable ($a_1, \ldots, a_4$ are larger) when r, e, and θ are small. We observe that when any of the r, e, and θ parameter increase they add more stress to the system and the effect of contingencies becomes larger. Therefore, the probability of an additional failure in the system increases (a_1, a_3, and a_4 decrease). We also observe that when any of r, e, or θ increase, the cascading failure enters the rapid escalation phase with smaller number of failures (a_2 decreases).

VII. Analysis of the SASE Model

Here, we analyze the SASE model by understanding the properties of the transition probability matrix $\mathbf{P}(t)$. To simplify the analysis, we first rearrange the indices of states in $\mathcal{S}$ by following three simple rules so that $\mathbf{Q}$ becomes upper diagonal matrix denoted by $\mathbf{Q}^d$. The three rules pertain the indices of states in $\mathbf{Q}^d$ such that: 1) $i < j$ if $F_i < F_j$; 2) $i < j$ if $F_i = F_j$ but $C_i^{\max} < C_j^{\max}$; and 3) $j = i+1$ if $F_i = F_j$ and $C_i^{\max} = C_j^{\max}$, but $I_i = 0$ and $I_j = 1$. Note that the SASE Markov chain is not

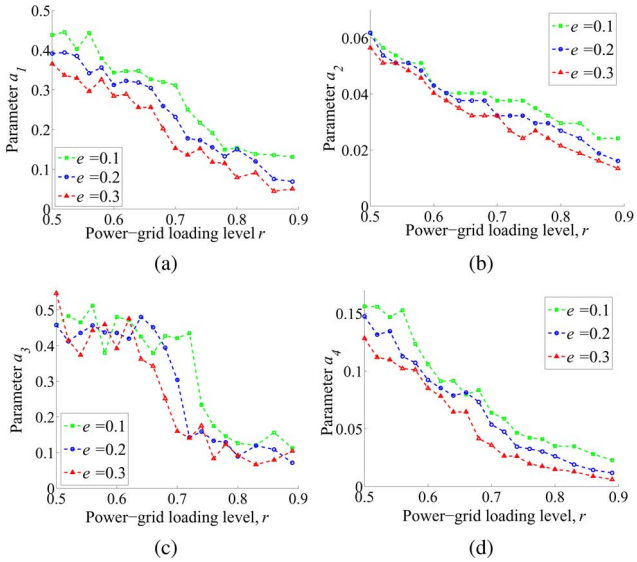

Fig. 9. SASE-model parameters (a) a_1, (b) a_2, (c) a_3, and (d) a_4 as a function of r parameterized by e.

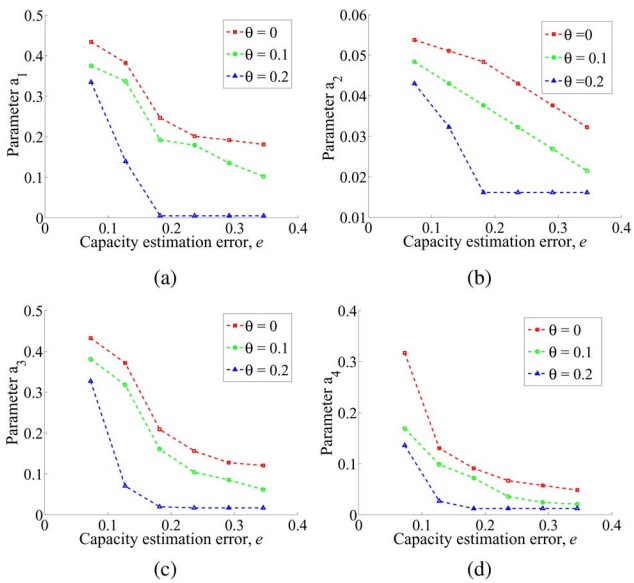

Fig. 10. SASE-model parameters (a) a_1, (b) a_2, (c) a_3, and (d) a_4 as a function of e parameterized by θ.

irreducible (and hence not ergodic) because $\mathbf{Q}^d$ is upper diagonal. This further implies that there is no stationary distribution for the SASE model and the canonical limit theorems of ergodic Markov chains are not applicable. Regardless, $\mathbf{P}(t)$ is governed by

$$\mathbf{P}'(t) = \mathbf{Q}^d \mathbf{P}(t) \tag{13}$$

where $\mathbf{P}'(t)$ denotes the matrix whose elements are time derivative of $p_{ij}(t)$ [17]. In principle, the solution of (13) is given by $\mathbf{P}(t) = e^{\mathbf{Q}^d t}\mathbf{P}(0)$. While the numerical solutions of $\mathbf{P}(t)$ can be easily obtained, to have better insight we pursue an analytical approach which can result in the asymptotic solution of $\mathbf{P}(t)$. To do so, the eigenvalues $\lambda_1, \lambda_2, \ldots, \lambda_N$ of $\mathbf{Q}^d$ and a complete system of associated right eigenvectors $\mathbf{u_1}, \mathbf{u_2}, \ldots, \mathbf{u_N}$ need to be determined. Then, $\mathbf{P}(t)$ can be represented as $\mathbf{P}(t) = e^{\mathbf{Q}^d t} = \mathbf{U}\Lambda(t)\mathbf{V}$, where $\mathbf{U}$ is the matrix whose column vectors are $\mathbf{u_1}, \mathbf{u_2}, \ldots, \mathbf{u_N}$ and $\mathbf{V} = \mathbf{U}^{-1}$. The matrix $\Lambda(t)$ is diagonal with $e^{\lambda_i t}$ as its ith diagonal element.

Due to the upper diagonal form of $\mathbf{Q}^d$ and by carrying out simple matrix manipulations, we can express $p_{ij}(t)$ as

$$p_{ij}(t) = \beta_{ij} + \sum_{i<k<j} \alpha_{ik} e^{\lambda_k t} \tag{14}$$

where $\beta_{ij} \triangleq \mathbf{U}(i,j)\mathbf{V}(j,j)$ and $\alpha_{ik} \triangleq \mathbf{U}(i,k)\mathbf{V}(i,k)$. Notice that $\mathbf{V}(j,j) = 1/\mathbf{U}(j,j)$ for $j = 1, 2, \ldots, N$. Since $\mathbf{Q}^d$ is upper diagonal λ_k is negative for all k, and hence $\lim_{t\to\infty} p_{ij}(t) = \beta_{ij}$.

Now, let $B(t, M \mid S_i)$ be the conditional probability of reaching a state with M or more failures by time t starting from an initial state S_i. The $B(t, M \mid S_i)$ can be obtained as follows:

$$B(t, M \mid S_i) = \sum_{n=M}^{m} \sum_{j\in\mathcal{J}_n} p_{ij}(t) \tag{15}$$

where $\mathcal{J}_n$ represents the set of indices of states with n failures, i.e., $\mathcal{J}_n \triangleq \{j : F_j = n\}$. The $B(t, M \mid S_i)$ estimates the evolution of the risk of cascading failures in time.

Further, using the asymptotic analysis, we can derive the conditional probability that a power grid *eventually* reaches a state with n failures from an initial state S_i defined as

$$D(n \mid S_i) \triangleq \sum_{j\in\mathcal{J}_n} \lim_{t\to\infty} p_{ij}(t) = \sum_{j\in\mathcal{J}_n} \beta_{ij}. \tag{16}$$

Hence, the probability mass function (PMF) of the blackout size, conditional on the initial state, can be computed by calculating $D(n \mid S_i)$ for $n = F_i, \ldots, m$.

VIII. Results

Here, we present results obtained from the SASE model applied to IEEE-118 bus system.

A. Conditional Blackout Probability

The PMF of the blackout size conditional on the initial state $D(n \mid S_i)$ is calculated using (16) and shown in Fig. 11 for a fixed initial state with $F_i = 2$ and $C_i^{\max} = 20$ MW. Fig. 11 also shows the effects of the operating characteristics of the power grid on $D(n \mid S_i)$. The results suggest that, when the power grid operates under a reliable operating configuration (small values of r, e and θ) the PMF of the blackout size has an exponential decay, which has also been observed empirically by Dobson (see Figs. 1, 2 in [12]) using real outage datasets [14]. On the other hand, when the power grid is stressed (large values of r, e and θ) the probability of large blackouts increases and a hump appears near the tail of the PMF. These conclusions from the analytical SASE model are confirmed by power-system simulation results as shown in Fig. 12. Note that the set of simulation results used to validate these conditional probabilities are different from the set of results used to identify the model parameters. All in all, these results validate that the SASE model with its low-dimensional, abstract state space is effective in capturing the dynamics of cascading failures in the power grid.

Note that the average size of cascading failures is approximately four in the scenario without stress [Fig. 12(a)] while

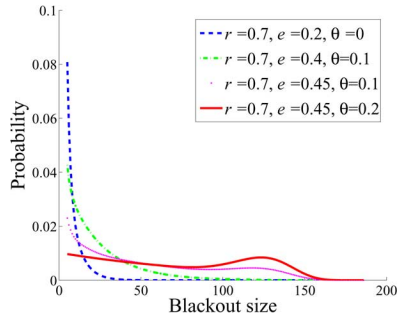

Fig. 11. Conditional PMF of the blackout size for four operating-characteristic settings and $F_i = 2$ and $C_i^{\max} = 20$ MW.

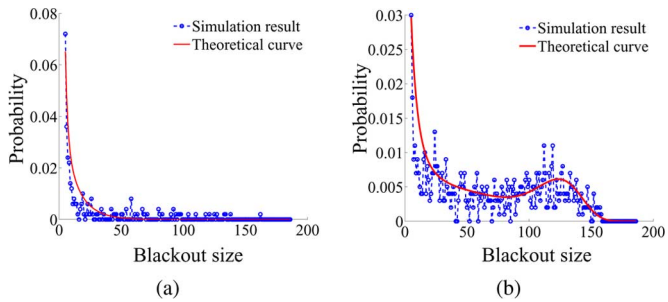

Fig. 12. Analytical and empirical conditional PMF of the blackout size (a) without stress, i.e., $r = 0.7, e = 0.25$ and $\theta = 0$, and (b) with stress, i.e., $r = 0.7, e = 0.35$ and $\theta = 0.2$, for the initial state with $F_i = 2$ and $C_i^{\max} = 20$ MW.

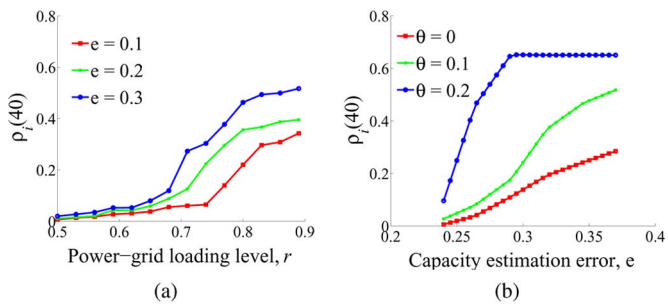

Fig. 13. Conditional blackout probability $\rho_i(M)$ for $M = 40$ as a function of (a) r parameterized by e and (b) e parameterized by θ for the initial state with $F_i = 2$ and $C_i^{\max} = 20$ MW.

this number is approximately 61 in the scenario with stress [Fig. 12(b)]. Therefore, one could use the SASE model to characterize the conditions for occurrence of large blackouts by identifying the operating characteristics that result in a hump in the tail of the PMF.

Next, consider the conditional probability of reaching a blackout state with at least M failures from an initial state S_i denoted by $\rho_i(M) \triangleq \sum_{n=M}^{m} D(n \mid S_i)$. For a fixed M and $F_i = 2$ and $C_i^{\max} = 20$ MW, the dependence of $\rho_i(M)$ on r and e is shown in Fig. 13(a) and on e and θ in Fig. 13(b). As expected, $\rho_i(M)$ increases with r, e, and θ. The results also suggest that at certain settings of the operating characteristics, a phase transition occurs in the blackout probability. This represents the critical operating settings for which the power grid becomes highly vulnerable to cascading failures.

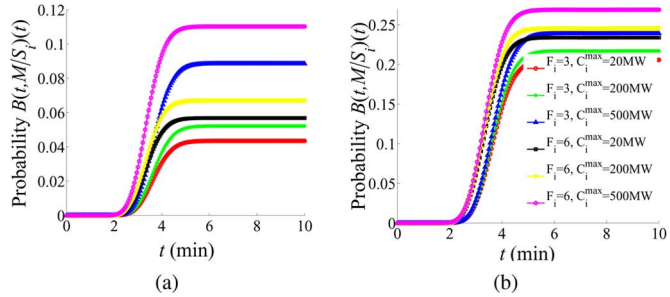

Fig. 14. Probability of reaching a blackout, $B(t, M \mid S_i)$, with $M = 30$ or more failures for $r = 0.7, e = 0.2, \theta = 0.1$, and initial states (a) with $F_i = 3$ and (b) with $F_i = 6$, and different values of $C_i^{\max}$.

B. Conditional Blackout Probability as a Function of Time

The numerical results of the conditional blackout probability $B(t, M \mid S_i)$ are calculated using (13) and (15). As a representative example, we have calculated $B(t, 30 \mid S_i)$ for $r = 0.7, e = 0.2$ and $\theta = 0.1$ for different initial states, S_i, as shown in Fig. 14. As the results show, the values of F_i and $C_i^{\max}$ associated with the initial state affect the evolution of the blackout probability. In particular, both the probability of reaching a power-grid state with M or more failures and its rate of change during escalation phase increase with F_i and $C_i^{\max}$. We reiterate that while we have assumed a single-line failure at a time in our model, the escalation phase in the cascading failure occurs as a result of shorter time between failures due to higher transition rates for such states (as the transition rates are state dependent). Also, note that $B(t, M \mid S_i)$ exhibits three phases. Interestingly, the three-phase theme of cascading failures were also seen in the behavior of the cascade-stop probability as well as the evolution of the accumulative number of failures.

C. Failure Evolution

Fig. 15 shows four realizations of the cascading-failure scenarios in terms of the evolution of the cumulative number of failures obtained using the SASE Markov chain. The initial state of the power grid in all the four realizations has two line failures with $C_i^{\max} = 80$ MW. Note that, in the realization with 163 eventual failures, the number of failures increases relatively gently at the beginning; however, failure of a line with large capacity at $t = 10$ min results in rapid increase in the number of failures in the power grid. In contrast, the number of failures in other realizations increases rapidly right from the beginning but they transit to stable state earlier as the value of $P_{\text{stop}}(S_i)$ in these cases is larger. Note that, from Fig. 15, we observe similar forms to those shown in Fig. 2 for the historical blackouts.

D. Size of the Cascading Failures

To assess the severity of cascading failures, we consider the number of subsequent failures induced by each initial failure. For a given initial state S_i with F_i initial failures, we define $R_{S_i} \triangleq (F_i - F_i^{\text{end}})/F_i$, where F_i^{end} is the random variable for the final number of failures in the power grid after cascading failure ends. Here, we study the mean of R_{S_i} as a metric representing the severity of cascading failures, which can be calculated as $\mathsf{E}[R_{S_i}] = \sum_{j=1}^{N} \lim_{t\to\infty} p_{ij}(t)(F_j - F_i)/F_i$. (For this metric to be meaningful, the initial number of failures F_i

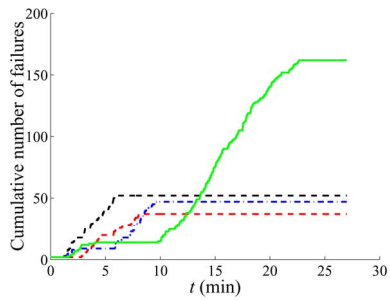

Fig. 15. Realizations of the evolution of the cumulative line failures using the SASE model for $r = 0.7, e = 0.2, \theta = 0.1, F_i = 2$, and $C_i^{\max} = 80$ MW.

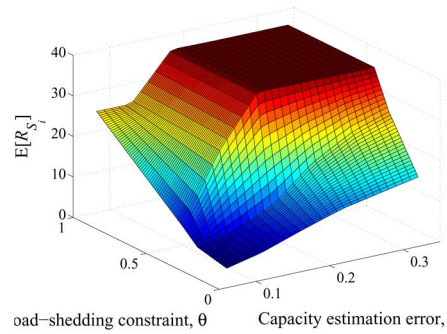

Fig. 16. $\mathsf{E}[R_{S_i}]$ for the IEEE 118-bus system as a function of load-shedding constraint level θ and the capacity estimation error e for $r = 0.7$ and the initial state with $F_i = 3$ and $C_i^{\max} = 20$ MW.

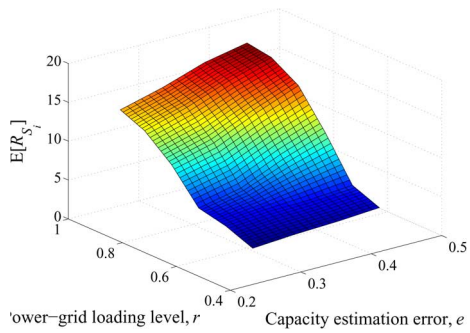

Fig. 17. $\mathsf{E}[R_{S_i}]$ for the IEEE 118-bus system as a function of the power-grid loading level r and the capacity estimation error e for $\theta = 0$ and the initial state with $F_i = 3$ and $C_i^{\max} = 20$ MW.

must be small, which in general is met in most real scenarios.) Figs. 16 and 17 show that $\mathsf{E}[R_{S_i}]$ (for $F_i = 3$) increases with r, e and θ. From results in Fig. 16, we observe that there is a critical value of load-shedding constraint level (approximately $\theta = 0.2$) above which strong cascading behavior is observed. Furthermore, this trend becomes more evident and aggressive as the capacity estimation error e increases. Similarly, the results in Fig. 17 suggests that there is a critical loading level (approximately $r = 0.8$) for which the rate of change in $\mathsf{E}[R_{S_i}]$ increases abruptly for all values of e. We reiterate that the *N-1* security has been ensured in all loading levels of the power grid; therefore, the initial contingency is assumed to have at least two initial failures.

IX. Conclusion

We have developed a scalable and analytically tractable probabilistic model, termed the stochastic abstract-state evolution model, which describes the dynamics of cascading failures based upon Markov chains. The state space of the SASE model is defined by a reduced, abstract state space that retains key physical attributes of the power grid. We have formulated the state-dependent transition rates associated with the SASE model in terms of key operating characteristics of the power grid including the power-grid loading level, transmission-capacity estimation error, and constraints in implementing load shedding. The temporal analysis of the SASE model and its asymptotic behavior together enable determining the probability mass function of the blackout size, the evolution of the blackout probability from a specific initial state, as well as assessing the severity of the cascading behavior as a function of various operating settings of the power grid. The SASE model also enables the identification of critical regions of the space of key power-grid operating characteristics for which severe cascading behavior may occur.

Appendix A
Derivation of (7)

We start by defining the following events: 1) E_{stop}, which is the event that cascade-stop transition occurs; 2) E_{F_i}, which is the event that the power grid has F_i failures; and 3) $E_{C_i^{\max}}$, which is the event that the maximum capacity of the failed lines in the power grid is $C_i^{\max}$. Note that $P_{\text{stop}}(S_i)$ is the conditional probability $\mathsf{P}\{E_{\text{stop}} \,|\, E_{F_i} \cap E_{C_i^{\max}}\}$. Next, we use the simple approach used in [26], in conjunction with certain reasonable assumptions to approximately represent $\mathsf{P}\{E_{\text{stop}} \,|\, E_{F_i} \cap E_{C_i^{\max}}\}$ in terms of a weighted superposition of $\mathsf{P}\{E_{\text{stop}} \,|\, E_{F_i}\}$ and $\mathsf{P}\{E_{\text{stop}} \,|\, E_{C_i^{\max}}\}$. We begin by noting that multiple application of Bayes rule yields

$$\mathsf{P}\left\{E_{\text{stop}} \,|\, E_{F_i} \cap E_{C_i^{\max}}\right\} = \frac{\mathsf{P}\left\{E_{\text{stop}} \cap E_{F_i}\right\} \mathsf{P}\left\{E_{C_i^{\max}} \,|\, E_{\text{stop}} \cap E_{F_i}\right\}}{\mathsf{P}\left\{E_{F_i} \cap E_{C_i^{\max}}\right\}}. \quad (17)$$

Using the representation in (17), we can write

$$\mathsf{P}\left\{E_{\text{stop}} \,|\, E_{F_i} \cap E_{C_i^{\max}}\right\} = \mathsf{P}\left\{E_{\text{stop}} \,|\, E_{F_i}\right\} \frac{\mathsf{P}\left\{E_{C_i^{\max}} \,\middle|\, E_{\text{stop}} \cap E_{F_i}\right\}}{\mathsf{P}\left\{E_{C_i^{\max}} \,\middle|\, E_{F_i}\right)\}}. \quad (18)$$

With a similar approach, we can also write

$$\mathsf{P}\left\{E_{\text{stop}} \,|\, E_{F_i} \cap E_{C_i^{\max}}\right\} = \mathsf{P}\left\{E_{\text{stop}} \,|\, E_{C_i^{\max}}\right\} \frac{\mathsf{P}\left\{E_{F_i} \,|\, E_{\text{stop}} \cap E_{C_i^{\max}}\right\}}{P(E_{F_i} \,|\, E_{C_i^{\max}}\}}. \quad (19)$$

Now, using (18) and (19), we can write

$$\begin{aligned}\mathsf{P}\left\{E_{\text{stop}} \mid E_{F_i} \cap E_{C_i^{\max}}\right\} &= w\mathsf{P}\left\{E_{\text{stop}} \mid E_{F_i}\right\} \frac{\mathsf{P}\left\{E_{C_i^{\max}} \mid E_{\text{stop}} \cap E_{F_i}\right\}}{\mathsf{P}\left\{E_{C_i^{\max}} \mid E_{F_i}\right\}} \\ &\quad + (1-w)\mathsf{P}\left\{E_{\text{stop}} \mid E_{C_i^{\max}}\right\} \frac{\mathsf{P}\left\{E_{F_i} \mid E_{\text{stop}} \cap E_{C_i^{\max}}\right\}}{P(E_{F_i} \mid E_{C_i^{\max}}\}}\end{aligned} \tag{20}$$

where $w \in [0,1]$. In this paper, $\mathsf{P}\{E_{\text{stop}} \mid E_{F_i}\}$ and $\mathsf{P}\{E_{\text{stop}} \mid E_{C_i^{\max}}\}$ are denoted by $P^{(1)}_{\text{stop}}(F_i)$ and $P^{(2)}_{\text{stop}}(C_i^{\max})$, respectively.

Next, we assume that the dependence of the event $E_{C_i^{\max}}$ on the event E_{stop} is weaker than the dependence of the event $E_{C_i^{\max}}$ on the event E_{F_i}, which implies that $\mathsf{P}\{E_{C_i^{\max}} \mid E_{\text{stop}} \cap E_{F_i}\} \approx \mathsf{P}\{E_{C_i^{\max}} \mid E_{F_i}\}$. This simplifying assumption can be justified from the physical characteristics of power grids. Based on our simulation results, we know that given that F_i is large, there is a high probability that $C_i^{\max}$ is also large; on the other hand, when F_i is small then the probability of having large $C_i^{\max}$ is small. For example, when F_i is large the probability of high capacity line failures increases due to high stress on the system and the large ratio of the number of high capacity lines to the total number of lines in the system. Therefore, although the knowledge of event E_{stop} adds information about the occurrence of the event $E_{C_i^{\max}}$ we assume that it does not significantly alter the probability distribution of the event $E_{C_i^{\max}}$ given E_{F_i}. Similarly to the previous assumption, we assume that the dependence of the event E_{F_i} on the event E_{stop} is weaker than the dependence of the event E_{F_i} on the event $E_{C_i^{\max}}$. Hence, when $C_i^{\max}$ is small then the probability of F_i being large is small and E_{stop} does not alter this probability significantly. These assumptions enable us to approximate (20) by (7).

REFERENCES

[1] I. Dobson, B. A. Carreras, V. E. Lynch, and D. E. Newman, "Complex systems analysis of series of blackouts: Cascading failure, critical points, and self-organization," *Chaos*, vol. 17, no. 2, 2007, Art. ID 026103.

[2] I. Dobson, B. A. Carreras, and D. E. Newman, "A loading-dependent model of probabilistic cascading failure," *Probabil. Eng. Inf. Sci.*, vol. 19, no. 1, pp. 15–32, 2005.

[3] M. Rahnamay-Naeini and M. M. Hayat, "On the role of power-grid and communication-system interdependencies on cascading failures," in *Proc. IEEE Global Conf. Signal Inf. Process.*, 2013.

[4] C. D. Brummitt, R. M. D'Souza, and E. A. Leicht, "Suppressing cascades of load in interdependent networks," in *Proc. Nat. Acad. Sci. USA*, 2012, vol. 109, no. 12, pp. E680–E689.

[5] I. Dobson, B. A. Carreras, and D. E. Newman, "Branching process models for the exponentially increasing portions of cascading failure blackouts," in *Proc. 38th Hawaii Int. Conf. Syst. Sci.*, Jan. 2005, p. 64a.

[6] M. Rahnamay-Naeini, Z. Wang, A. Mammoli, and M. M. Hayat, "A probabilistic model for the dynamics of cascading failures and blackouts in power grids," in *Proc. IEEE Power and Energy Soc. Gen. Meeting*, Jul. 2012, pp. 1–8.

[7] Z. Wang, A. Scaglione, and R. J. Thomas, "A Markov-transition model for cascading failures in power grids," in *Proc, 45th Hawaii Int. Conf. Syst. Sci.*, Jan. 2012, pp. 2115–2124.

[8] R. Baldick *et al.*, "Initial review of methods for cascading failure analysis in electric power transmission systems," in *Proc. IEEE Power and Energy Soc. Gen. Meeting-Conversion and Delivery of Electrical Energy in the 21st Century*, 2008, pp. 1–8.

[9] P. Hines, E. Cotilla-Sanchez, and S. Blumsack, "Topological models and critical slowing down: Two approaches to power system blackout risk analysis," in *Proc. 44th Hawaii Int. Conf. Syst. Sci.*, 2011, pp. 1–10.

[10] C. L. DeMarco, "A phase transition model for cascading network failure," *IEEE Control Syst. Mag.*, vol. 21, no. 6, pp. 40–51, Jun. 2001.

[11] H. Ren and I. Dobson, "Using transmission line outage data to estimate cascading failure propagation in an electric power system," *IEEE Trans. Circuits Syst. II, Exp. Briefs*, vol. 55, no. 9, pp. 927–931, Sep. 2008.

[12] I. Dobson, "Estimating the propagation and extent of cascading line outages from utility data with a branching process," *IEEE Trans. Power Syst.*, vol. 27, no. 4, pp. 2146–2155, Nov. 2012.

[13] North American Electric Reliability Council, Princeton, NJ, USA, "NERC 1992–2009 System Disturbances Reports," 2009.

[14] Bonneville Power Administration Transmission Services Operations and Reliability [Online]. Available: http://transmission.bpa.gov/Business/Operations/Outages

[15] U.S.-Canada System Outage Task Force, Princeton, NJ, USA, "Final Report on the August 14th Blackout in the United States and Canada 2004.

[16] J. D. Glover, M. S. Sarma, and T. J. Overbye, *Power System Analysis and Design*, 4th ed. Stamford, CT, USA: Cengage Learning, 2008.

[17] S. Karlin and H. Taylor, *A First Course in Stochastic Processes*, 2nd ed. New York, NY, USA: Academic, 1975.

[18] A. J. Wood and B. F. Wollenberg, *Power Generation, Operation, and Control*, 2nd ed. New York, NY, USA: Wiley, 1996.

[19] Q. Chen and L. Mili, "Composite power system vulnerability evaluation to cascading failures using importance sampling and antithetic variates," *IEEE Trans. Power Syst.*, vol. 28, no. 3, pp. 2321–2330, Aug. 2013.

[20] M. Bockarjova and G. Andersson, "Transmission line conductor temperature impact on state estimation accuracy," *IEEE Lausanne Power Tech.*, 2007.

[21] R. Ptzner, K. Turitsyn, and M. Chertkov, "Controlled tripping of overheated lines mitigates power outages," Rep. arXiv:1104.4558v2, 2011.

[22] J. Chen, J. S. Thorp, and I. Dobson, "Cascading dynamics and mitigation assessment in power system disturbances via a hidden failure model," *Int. J. Electr. Power Energy Syst.*, vol. 27, no. 4, pp. 318–326, 2005.

[23] M. Rahnamay-Naeini, Z. Wang, A. Mammoli, and M. M. Hayat, "Impacts of control and communication system vulnerabilities on power systems under contingencies," in *Proc. IEEE Power Energy Soc. Gen. Meeting*, Jul. 2012, pp. 1–7.

[24] R. D. Zimmerman, C. E. Murillo-Sanchez, and R. J. Thomas, "MATPOWER: Steady-state operations, planning, and analysis tools for power systems research and education," *IEEE Trans. Power Syst.*, vol. 26, no. 1, pp. 12–19, Feb. 2011.

[25] M. J. Eppstein and P. Hines, "A random chemistry algorithm for identifying collections of multiple contingencies that initiate cascading failure," *IEEE Trans. Power Syst.*, vol. 27, no. 3, pp. 1698–1705, Aug. 2012.

[26] A. G. Journel, "Combining knowledge from diverse sources: An alternative to traditional data independence hypotheses," *Math. Geol.*, vol. 34, no. 5, pp. 573–596, 2002.

Mahshid Rahnamay-Naeini (S'13) received the B.Sc. degree in computer engineering from Sharif University of Technology, Tehran, Iran, in 2007, and the M.Sc. degree from Amirkabir University of Technology (Tehran Polytechnic), Tehran, in 2009. She is currently working toward the Ph.D. degree in electrical and computer engineering department at the University of New Mexico, Albuquerque, NM, USA.

Her research interests include reliability and performance analysis of communication networks, smart grids and smart-grid networking, cyber-physical infrastructure design, and resource management in distributed systems.

Zhuoyao Wang received the B.S. degree from Jilin University, Jilin, China, in 2008, and the M.S. degree in electrical and computer engineering from the University of New Mexico, Albuquerque, NM, USA, in 2011, where he is currently working toward the Ph.D. degree.

His research is focused on distributed and networked computing with applications to cloud computing and smart grids.

Nasir Ghani (SM'13) received the Ph.D. degree in computer engineering from the University of Waterloo, Waterloo, ON, Canada.

He is a Professor with the Electrical Engineering Department, University of South Florida, Tampa, FL, USA. Earlier he was a Member of Faculty and Associate Department Chair with the Electrical and Computer Engineering Department, University of New Mexico, Albuquerque, NM, USA. He has also spent over eight years in industry working at several large corporations (Nokia, IBM, and Motorola) and startups. He is involved in a range of research activities in cyber infrastructure design, disaster recovery, cloud computing, and cyber-physical systems. His research has been supported by the National Science Foundation, Defense Threat Reduction Agency, Department of Energy, Qatar Foundation, Department of Education, NSWC, and Sprint-Nextel Corp.

Prof. Ghani was the recipient of the National Science Foundation CAREER Award in 2005. He has chaired the IEEE ComSoc Technical Committee on High Speed Networks from 2008 through 2010 and has been a symposium co-chair for various IEEE conferences.

Andrea Mammoli (M'12) received the B.Eng. and Ph.D. degrees from the Department of Mechanical and Materials Engineering, University of Western Australia, Crawley, Australia.

He is Professor of mechanical engineering and Director of the University of New Mexico (UNM) School of Engineering's Center for Emerging Energy Technologies, Albuquerque, NM, USA. He also holds a secondary appointment with the Department of Electrical and Computer Engineering at UNM. After two years as a Director-funded Postdoctoral Fellow with Los Alamos National Laboratory, in 1997, he joined the UNM as a Research Assistant Professor. Until 2004, he conducted research in the flow of heterogeneous materials, using both experimental techniques (nuclear magnetic resonance, particle image velocimetry and rheometry) as well as high-performance direct numerical simulation using primarily boundary element techniques. Stimulated by a DOE-sponsored project on CO2 sequestration, and by a sabbatical year at the Università Politecnica delle Marche in Italy, in 2005, he steered his research activities to the area of energy systems, beginning with a project to refurbish and modernize the solar-assisted HVAC in the UNM Mechanical Engineering building. This initial effort spun off many related projects, dealing with the interaction between buildings and the electric power grid, especially concerning how buildings can enable higher levels of renewable energy from all sources. He collaborates with the utility industry and national laboratories (Sandia, Berkeley and Los Alamos) on various demonstration projects and testbeds to bring new technologies online speedily.

Majeed M. Hayat (F'14) was born in Kuwait in 1963. He received the B.S. degree (*summa cum laude*) in electrical engineering from the University of the Pacific, Stockton, CA, USA, in 1985, and the M.S. and Ph.D. degrees in electrical and computer engineering from the University of Wisconsin-Madison, Madison, WI, USA, in 1988 and 1992, respectively.

He is currently a Professor of electrical and computer engineering, Associate Director of the Center for High Technology Materials, and General Chair of the Optical Science and Engineering Program at the University of New Mexico, Albuquerque, NM, USA. His research activities cover a broad range of topics including avalanche photodiodes, signal and image processing, algorithms for spectral and radar sensing and imaging, optical communication, networked computing, and modeling interdependent networks with applications to smart grids. He was an associate editor of *Optics Express* from 2004 to 2009. He has authored or coauthored over 85 peer-reviewed journal articles (over 2800 citations, $\mathrm{H\text{-}Index} = 28$) and has eight issued patents, three of which have been licensed.

Dr. Hayat is Fellow of the International Society of Optical Engineering and the Optical Society of America. He was Chair of the topical committee of Photodetctors, Sensors, Systems and Imaging within the IEEE Photonics Society from 2010 to 2013. He was the recipient of the National Science Foundation Early Faculty Career Award (1998) and the Chief Scientist Award for Excellence (2006) by the National Consortium for MASINT Research of the Defense Intelligence Agency.